Highlights

- Core-shell structured TiO_2-SiO_2 nanoparticles of varying shell thickness were synthesized as photo-killing agents.
- The effect of the silica shell thickness on the photoreactivity, cytotoxicity, haemocompatibility and photo-killing ability of the TiO_2 nanoparticles was investigated.
- Strong photo-killing effect and enhanced cytocompatibility were achieved by controlling the silica shell thickness to 5.5 nm.

***Graphical Abstract (for review)**

Graphical abstract:

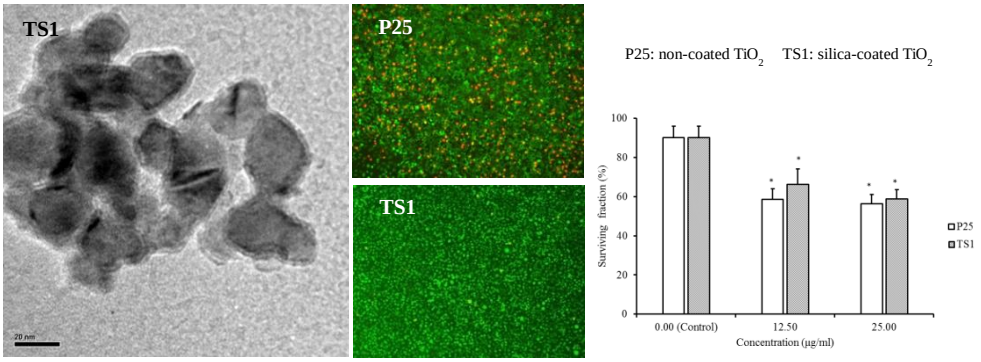

TEM image of core-shell structured TiO_2-SiO_2 nanoparticles (TS1) (Left), showing enhanced compatibility to L929 cells (Middle) and effective killing ability of the cells upon photoexcitement (Right), in comparison with the control nanoparticles (P25).

Controlling silica coating thickness on TiO_2 nanoparticles for effective photodynamic therapy

Xiaohui Feng[a‡], Shaokun Zhang[b‡], Xia Lou[a*]

[a] Department of Chemical Engineering, Curtin University, WA 6102 Australia

[b] Department of Orthopedics, The First Hospital of Jilin University, China

[‡] These authors contributed equally to this work.

*Corresponding author. Tel.: +61892661682; fax: +61892662681.
Email address: X.Lou@curtin.edu.au.

ABSTRACT

Photosensitive nanoparticles are useful in developing phototherapeutic agents for targeted cancer therapy. In this paper, core-shell structured titanium dioxide-silica (TiO_2-SiO_2) nanoparticles, with varying shell thickness, were synthesized. The influence of the silica shell thickness on the photoreactivity, cytotoxicity and photo-killing ability of the TiO_2 nanoparticles was investigated. Silica coating reduced the photocatalytic reactivity but improved the cytocompatibility of the TiO_2 nanoparticles. This effect was amplified with increasing silica shell thickness. When the silica thickness was about 5.5 nm, the coated TiO_2 not only retained a high level photodynamic reactivity, comparable to the non-coated TiO_2 nanoparticles, but also demonstrated an improved cell compatibility and effective photo-killing ability upon the mouse fibroblast cells (L929).

Keywords: Silica-coated TiO_2 nanoparticles; Silica coating; TiO_2 nanoparticles; Photo-killing agent; Photodynamic therapy

1. Introduction

Nanoparticles of TiO_2 have attracted increasing attention in life sciences since the first report of photocatalytic disinfection by Matsunaga et al. in 1985 [1]. When being irradiated by ultraviolet (UV), the TiO_2 nanoparticles can be photoexcited to produce a negative electron (e^-_{CB}) in the conduction band and a positive hole (h^+_{VB}) in the valence band. In an aqueous environment, the photo-induced electrons and hole pairs react with oxygen or water to generate reactive oxygen species (ROS) such as hydroxyl (HO·) and superoxide radical ($\cdot O_2^-$). These reactive species are powerfully oxidative and can destroy the structure of various organic molecules, therefore, having found extensive applications in the removal of infectious molecules and organic pollutants. TiO_2 nanoparticles also have been regarded as a potential photosensitizing agent for photodynamic therapy (PDT) [2-5]. The ROS generated from the photoexcited TiO_2 nanoparticles can react with cell membranes and cell interiors, leading to toxic responses and/or death of cells [6]. Many investigations on photodecomposition of tumour cells have been undertaken recently. Cai et al. reported that TiO_2 nanoparticles completely killed HeLa cells with UV irradiation [7]. Stefanous et al. also indicated that photoexcited TiO_2 nanoparticles efficiently inhibited the aggregation of platelets, which led to discontinuation of haematogenous metastasis [8]. The photo-killing effect of nitrogen-doped TiO_2 nanoparticles in the visible region also has been reported [9]. The research mostly has been limited to lab investigations. The clinical application of TiO_2 nanoparticles has been hampered by problems such as insufficient selectivity and low efficiency resulting from the lack of cell-specific accumulation of TiO_2 on cancer cells [10]. In addition, the metal ions exposed on the surfaces of nanoparticles can lead to metal toxicity in cells [10, 11]. The insolubility of TiO_2 in water is also a problem as the nanoparticles tend

to aggregate in a physiological environment, leading to a reduction of surface area and reactivity of the particles [12, 13].

Coating nanoparticles with silica, using tetraethoxysilane in the presence of ammonia, has been used widely to improve the dispersion and the cell compatibility of various nanoparticles in a physiological environment [14-16]. The method is simple and can be operated at ambient temperature. The resultant nanoparticles consist of a core made of the base nanoparticle and a shell made of silica, therefore, known as a core-shell structure. Silica, as a shell, can act as a protector to reduce the influence of the outer environment upon the core nanoparticles. Since the silica surface is electrostatically stable, it also improves the dispersion of the core nanoparticles [17]. Although the overall particle stability and dispersibility can be improved after silica coating, the properties of the core component, such as reactivity and thermal stability, also may be modified [18, 19]. This article presents our investigations regarding the influence of the silica coating on the photoreactivity, the cytotoxicity and the photo-killing ability of TiO_2 nanoparticles. Silica-coated TiO_2 nanoparticles were synthesised at room temperature via Stöber method using commercially available TiO_2 nanoparticles (Degussa P25) and tetraethoxysilane (TEOS) as reactants. The silica shell thickness was finely tuned through alteration of the TiO_2-to-TEOS ratio in the reaction mixture. The obtained core-shell structured nanoparticles were examined using a field emission scanning electron microscope (FESEM), a transmission electron microscope (TEM) equipped with an energy dispersive spectroscope (EDS), and a Fourier transform infrared (FTIR) spectroscope. The photoreactivity of the silica-coated and non-coated TiO_2 nanoparticles was first examined through the photo-degradation of phenol, a compound that can be degraded into carbon dioxide, water and corresponding mineral acids in the presence of photocatalysts under UV light [20]. Cytotoxicity and haemocompatibility were also assessed. Following these examinations, silica-coated TiO_2 nanoparticles with an optimal

shell thickness, having retained good photoreactivity, were selected for the photo-killing effect investigation. The results are being used in the development of a targeted photodynamic nanosystem for cancer cells.

2. Experiment

2.1. Materials and chemicals

Degussa P25 (TiO_2 nanoparticles consisting of 80% anatase and 20% rutile) was purchased from Degussa. The average size of the nanoparticles was 25 nm. Tetraethoxysilane (TEOS) (99.999%), ammonia aqueous solution (4.13%) and ethanol (99.5%) were purchased from Sigma-Aldrich. All chemicals were reagent grade and used without further purification. Deionized water was used in this investigation.

2.2. Synthesis of TiO_2-SiO_2 core-shell nanoparticles

To a mixture of deionized water (20 ml) and ethanol (60 ml), 0.5 g P25 and 1.0 ml ammonia solution were added. The mixture was dispersed using ultrasonic vibration for about 30 min. Twenty ml of ethanol, containing various concentrations of TEOS, was added, dropwise, to the dispersion. This took about 30 min. The concentrations of TEOS added into the dispersion were 8.97 mM, 17.93 mM, 26.90 mM and 36.0 mM. These concentrations yielded theoretical molar ratios of Si/Ti of 0.14, 0.29, 0.43 and 0.57 in the products, respectively. After stirring for 2 h, the reaction mixtures were centrifuged at 7500 rpm for 5 min. The liquid in the centrifuge tube was removed and the resultant silica-coated TiO_2

nanoparticles were washed with ethanol (three times) to remove the excess amount of reactants and then dried overnight at room temperature under vacuum. The silica-coated TiO_2 nanoparticles were denoted as TSX (X=1, 2, 3 and 4). The reaction is shown in Scheme 1.

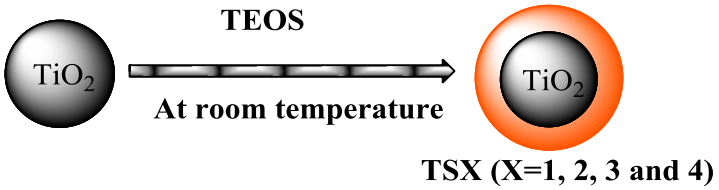

Scheme 1. The schematic representation of TiO_2 to silica-coated TiO_2 via the TEOS hydrolysis and condensation reaction. The theoretical molar ratios of Si/Ti in TS1-4 were 0.14, 0.29, 0.43 and 0.57, respectively.

2.3. Characterization of TiO_2-SiO_2 core-shell nanoparticles

FTIR analysis was conducted on a Perkin-Elmer Spectrum 100 using the KBr pellet technique at room temperature. The samples were mixed with dried KBr, using a mortar and pestle, and then the mixture was pelletized under vacuum. All the spectra were recorded in the range of 4000-400 cm^{-1} at a resolution of 4 cm^{-1}. FESEM (Zeiss Neon 40EsB FIB-SEM) was used to examine the morphology of P25 and the obtained TiO_2-SiO_2 nanoparticles. The samples were dispersed in deionized water using ultrasonic vibration and the solutions were deposited onto an aluminium stub where a platinum coating (2 nm) was applied as a conducting material. FESEM images of the nanoparticles were recorded at an accelerating voltage of 5 kV. The size of the nanoparticles was measured using the in-built Zeiss operational software, SmartSEM, that is linked to the magnification bar of the obtained images. The detailed morphology and chemical composition of the nanoparticles were further examined using TEM (JEOL JSM 2011) equipped with an energy dispersive spectroscope (EDS). Prior to the TEM examination, the nanoparticles were dispersed in ethanol using ultrasonic vibration with an approximate concentration of 10 µg/ml. They were then distributed on carbon-coated copper grid for examination.

2.4. Photoreactivity study

Examination of the photoreactivity of the produced core-shell nanoparticles was conducted in a 1L double-jacket reactor, as shown in scheme 2. A water bath was connected to the reactor through a pump to maintain the reaction temperature at 25± 0.5 °C and a magnetic stirrer was used for mixing. The UV irradiation was facilitated by a MSR 575/2 metal halide lamp (575 W, Philips) with the wavelength in a range of 315 to 1050 nm. In brief: a preferred amount of P25 and TSX (X=1, 2, 3, 4) was added to 200 ml of aqueous phenol solution and stirred for 30 min in the dark to obtain a homogeneous solution. Then the light was immediately switched on. At set time intervals, 3 ml of solution was withdrawn by a syringe and filtered using a 0.45 μm Millipore film. The concentration of phenol in the withdrawn samples was measured using a HPLC (Varian) with a UV-detector at the wavelength of 270 nm. The column was C-18 and the mobile phase was 30% acetonitrile and 70% deionized water. The amount of P25 used for photocatalytic reaction was 0.2 g resulting in a concentration of 1.0 g/L. To maintain the same concentration for TiO_2, the added amounts of TS1-4 were 0.22 g, 0.24 g, 0.26 g and 0.28 g, respectively.

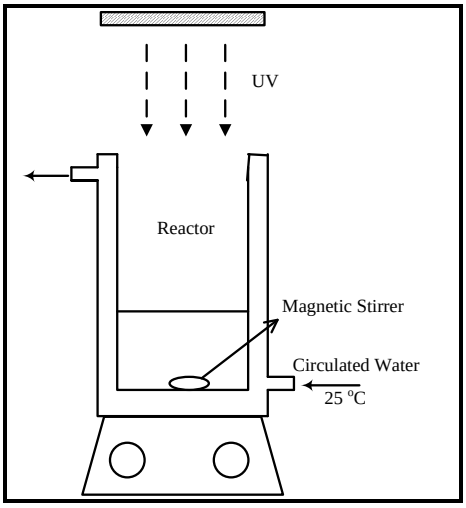

Scheme 2. Photocatalytic reaction set-up

2.5. Cell culture and nanoparticle preparation

Primary adherent mouse fibroblast connective tissue cells (L929) were purchased from ATCC (USA). The cells were cultured in Dulbecco's modified Eagle's medium (DMEM, Invitrogen, USA) supplemented with 10% fetal bovine serum (FBS, Sigma Aldrich). The cells were maintained at 37 ^{o}C in a humidified incubator with 5% CO_2 and 95% air. Nanoparticles of P25, TS1 and TS4 were suspended in phosphate buffered saline (PBS), each at concentrations of 12.5, 25, 50, 100 and 200 μg/ml, for further investigation.

2.6. Cytotoxicity study

The cell cytotoxicity was measured using the 3-(4, 5-dimethylthiazol-2-yl)-5-(3-cayboxymethoxyphenyl)-2-(4-sulfophenyl)-2H-tetrazolium (MTS) assay [21]. Briefly, L929 cells were plated at a density of $1x10^4$ cells per well in a 96-well plate in 200 μl of medium and incubated at 37 ^{o}C in 5% CO_2 atmosphere. After overnight incubation, the medium in the wells was replaced with fresh medium, described previously, containing the nanoparticles at

concentrations of 12.5, 25, 50, 100 and 200 µg/ml. A control experiment was conducted using cells treated with complete medium containing no nanoparticles. After 6 h and 24 h of incubation at 37 ^{o}C under 5% CO_2, the cell culture medium was removed and the plate was washed with PBS three times. 200 µL of MTS reagent was subsequently added to each well and the cells were incubated for 3 h under the same conditions. After the treatment, the absorbance of formed formazan at 490 nm was measured by microplate reader. The cell viability was calculated using the following equation [22]:

$$Cell\ viability = \frac{OD_{490}(sample)}{OD_{490}(control)} \times 100\% \quad (1)$$

where OD_{490} (sample) is the optical density of cells treated with various concentrations of nanoparticles and OD_{490} (control) is the optical density of cells incubated with medium only.

All the experiments were performed in triplicate in the dark. Cell morphology was photographed at the two time intervals using an Olympus BX61 microscope. The magnification was set at 5× for all samples.

2.7. Haemolysis assay

Fresh blood was obtained from a rabbit. Red blood cells (RBCs) were isolated from plasma using a refrigerated centrifuge at 1500 rpm for 15 min at 4 ^{o}C. The RBCs were further washed three times with sterile PBS by centrifugation until the supernatant was clear. Then 100 µl of the obtained particle suspensions in PBS at concentrations of 12.5, 25, 50,100 and 200 µg/ml were added to 100µl of the RBCs suspension. The mixtures were incubated at 37 °C for 1 h under constant shaking, and subsequently centrifuged at 1500 rpm for 15 min.

After the treatment, 100 µl of supernatant from each centrifuge tube was used to analyse haemoglobin release by microplate reader at the wavelength of 576 nm. Control experiments were performed under the same experimental conditions. 100 µl of the RBCs suspension was added to 100 µl of PBS as a negative control and to 100 µl of 0.5 % Triton X-100 as a positive control. The percentage haemolysis was calculated using the following equation [23]:

$$Hemolysis(\%) = \frac{OD_{576Sample} - OD_{576Negativecontrol}}{OD_{576PositiveControl} - OD_{576Negativecontrol}} \times 100\% \quad (2)$$

where $OD_{576\ sample}$, $OD_{576\ Negative\ control}$ and $OD_{576\ Positive\ control}$ are the optical densities of haemoglobin released from RBCs treated with, respectively, nanoparticles, PBS buffer and medium containing 0.5 % Triton X-100.

2.8. Photo-killing effect

The photo-killing effect of TiO_2-SiO_2 nanoparticles on L929 cells was examined as follows. L929 cells, at the density of $1x10^4$ cells per well, were seeded in a 96-well plate in RPMI-1640 medium (Lonza) and incubated overnight, in the dark, with 5% CO_2 and humidified atmosphere. Then the medium was replaced with the medium containing P25 or TS1 nanoparticles, each at concentrations of 12.5 and 25 µg/ml. A control experiment was conducted using cells treated with the medium containing no particle. After 24 hours, the cells were exposed to UV light (365nm, 50W) for 20 min. The cells were incubated for another 24 h in the dark and then the viability of the cells was tested using the MTS assay as described above. The cell viability was expressed as the ratio of the number of viable cells remaining after UV irradiation to those present in the samples without UV irradiation.

2.9. Statistical analysis

The experimental data of the aforementioned cellular work were analysed utilizing the student's T-test and the results were presented as mean ± standard deviation. The standard deviation values are expressed as error bars. Statistical significance was considered at a probability of $p < 0.05$.

3. Results and Discussion

3.1. Characterization of P25 and TS1-4

Four core-shell structured TiO_2-SiO_2 nanoparticles, TS1, TS2, TS3 and TS4, were synthesized via the Stöber method using varying ratios of P25 and tetraethoxysilane (TEOS). FESEM images showed that the resultant nanoparticles were sphere-like and slightly bigger than P25 (Fig. 1). The analysis of 30 particles from each of the FESEM images indicated that the non-coated TiO_2 (P25) had a mean diameter of 24±1 nm, which is in agreement with the product specification provided by the supplier. The coated particles were about 35±2 nm, 39±1 nm, 42±2 nm and 46±2 nm for TS1, TS2, TS3 and TS4 respectively, indicating an increased shell thickness of 5.5 nm, 7.5 nm, 9 nm and 11 nm in TS1-4. The gradual increase in the particle size, and therefore the shell thickness, was due to the increase of TEOS concentration (Si/Ti ratio) in the reaction mixtures.

The TEM micrographs in Fig. 2 (Left) further demonstrated the core-shell structure of the TiO_2-SiO_2 nanoparticles. EDS analysis of TS1 indicated the presence of silica on the surface

of the TiO_2 nanoparticles (Fig. 2 Right). Further analysis of these nanoparticles using FTIR, shown in Fig. 3, confirmed the formation of the silica network through the strong adsorption peaks at 1065 and 1180 cm^{-1} which correspond to the asymmetric Si-O-Si bending and stretching vibration, respectively. The peak at 1625 cm^{-1} is attributed to O-H bending vibration of the surface silanol group of the silica gel (-Si-O-H groups). There is also a weak adsorption peak at 950 cm^{-1}, attributed to the flex vibrations of Si-O-Ti, indicating that the TiO_2 core is connected with the silica shell through a chemical bond [24]. The weak peaks at 2920 and 2853 cm^{-1} arise from the symmetric and asymmetric stretching vibrations of the $-CH_2$ and $-CH_3$ groups, which indicate the presence of the intermediate reaction product $(OR)_3Si(OH)$ (R= $-CH_2CH_3$) (Scheme 3) [25]. As shown in Fig. 3, these peaks are generally stronger in the coated TiO_2 containing the higher silica component. The strong signals at approximately 650 and 500 cm^{-1} are due to the Ti-O stretching vibration, confirming the presence of TiO_2 in the nanoparticles [26, 27].

$$Si(OR)_4 + H_2O \xrightarrow{OH^-} (OR)_3Si(OH) + ROH$$

$$(OR)_3Si(OH) + H_2O \longrightarrow SiO_2 + 3ROH$$

Scheme 3. The hydrolysis reaction of TEOS and the subsequent condensation of the intermediate reaction product of $(OR)_3Si(OH)$ [28].

3.2. Photocatalytic reactivity of P25 and TS1-4

The photodegradation reaction of phenol was carried out in the presence of P25 and TS1-4, using a concentration that was equivalent to 1.0 g/L P25. As shown in Fig. 4, 94.5% of phenol was degraded after 60 min of irradiation when P25 was used. When TS1-4 were used,

the phenol degradation yields were reduced to 86.6, 58.7, 50.5 and 36.7%, respectively, indicating a reduction in photocatalytic reactivity of the coated TiO_2 nanoparticles. The apparent degradation rate constant of these nanoparticles was estimated using the Langmuir-Hinshelwood equation [29]:

$$\ln \frac{c}{c_o} = -\kappa t \tag{3}$$

where *k* is apparent reaction rate constant in the unit of time^{-1}, C_0 is the initial concentration and C is the concentration at time t.

The computed *k* values for P25, TS1, TS2, TS3 and TS4 were 0.0498, 0.0351, 0.0152, 0.0113 and 0.0075 min^{-1}, indicating a rapid decrease in the photo-degradation rate with increase in shell thickness (Fig. 4 insert). The reduced photo-catalytic reactivity can be attributed to the shielding effect of the silica shell formed on the surface of TiO_2 nanoparticles. That is to say that the silica shell acted as a barrier to prevent the migration of reactive radicals to the surface of the nanoparticles, which led to a decrease of active radicals $O_2^{\bullet -}$ and $OH\bullet$ for the oxidation of phenol [18].

It should be noted that the calculation was carried using the experimental data up to 60 min. The least squared R values for each fitting were 0.95, 0.99, 0.99 and 0.96. When the reaction was extended to 90 min, phenol degradation results for P25, TS1, TS2, TS3 and TS4 were 99.9, 97.6, 87.5, 78.7 and 58.9%, respectively. This indicates that, with a slight increase in reaction time, TS1 (with a shell thickness of 5.5 nm), is able to yield a complete photo-degradation of phenol, similar to P25. Based on these observations, TS1, TS4 and P25 nanoparticles were selected for the cytotoxicity, haemocompatibility and photo-killing investigations.

3.3. Cytotoxicity and haemocompatibility of P25, TS1 and TS4

The MTS assay was employed to determine the viability of L929 cells treated with P25 (the non-coated TiO_2 nanoparticles), TS1 and TS4 (the silica-coated TiO_2 nanoparticles) of varying concentrations (12.5, 25, 50, 100 and 200 μg/ml). The culture was carried out in dark for various time intervals. Results are shown in Fig. 5. When the nanoparticle concentration was below 200 μg/ml, the viability was generally the same for both untreated cells and cells treated with P25, TS1 and TS4. Incubation for 6 hours or 24 hours did not make any difference. When the concentration of nanoparticles was increased to 200 μg/ml, no significant difference in cell viability was observed at 6 hours. However, when the incubation time was extended to 24 hours, the P25-treated cell viability was reduced to 82.0% (relative to control) ($p<0.05$), whilst the TS1- and TS4-treated cell viability was 96.5% and 100%, suggesting a much lower cytotoxicity of the silica-coated nanoparticles. This can be attributed to the silica coating being cytocompatible. The optical micrographs (Fig.6) of the P25-treated cells, the TS1-treated cells and the TS4-treated cells at 24 h further confirm the results obtained from the MTS assay. As shown in Fig. 6(b), there was a portion of red-stained nuclei in the cell culture, indicating that the cells had undergone apoptosis after exposure to P25 nanoparticles. However, under the same conditions, there were scarce red-stained nuclei in both control cells (Fig. 6(a)) and those treated with TS1 and TS4 nanoparticles (Fig.6(c) and 6(d)). A similar result was reported by Mbeh et al. [16] in a biocompatibility study of silica-coated magnetite nanoparticles. They have concluded that a silica shell significantly reduced the cellular toxicity of pure magnetite nanoparticles.

In vitro haemolysis assays of P25 and TS1 were conducted at the same concentration range. Triton X-100 was used to induce full haemoglobin release. As shown in Fig. 7, the

haemolysis percentage was well below 5.0% across the range of investigated concentrations. This indicates that P25, TS1 and TS4 exhibit excellent haemocompatibility and can be further used *in vivo*.

3.4. Photo-killing effect of P25 and TS1

In order to select an appropriate UV exposure time, the effect of UV irradiation on L929 cell viability was first tested. Fig. 8 shows that the surviving fraction of L929 cells generally decreased with increasing irradiation time. When the irradiation time was over 40 min, the surviving fraction of L929 cells was only 15.5%, suggesting UV irradiation is harmful to L929 cells. At 20 min, the surviving fraction of L929 cells was 90.2%, showing a small suppression in cell proliferation. Based on these results, the photo-killing effect of P25 and TS1 nanoparticles were evaluated through the comparison of the viability of non-treated cells, with that of cells treated with P25 or TS1, after UV irradiation for 20 min. As shown in Fig. 9, the viability of the L929 cells was 90.2% relative to that of cells without exposure to the UV light. However, the viability of L929 cells was reduced to 58.6% and 66.3% in the presence of 15 μg/ml of P25 and TS1, and further to 56.5% and 58.9% when the concentration of the nanoparticles was increased to 25 μg/ml. In comparison to the untreated cells, a statistically significant ($p<0.05$) photo-killing effect of both P25 and TS1 on L929 cells was demonstrated. P25 was slightly more powerful in killing the L929 cells at 12.5 μg/ml. However the killing effect became almost the same ($p \approx 0.05$) when the nanoparticle concentration was increased to 25 μg/ml. It should be noted that the relative concentration of TiO_2 in TS1 is 90% of the apparent concentration in this experiment. These results further suggest that TS1 and P25 exhibit a similar photo-killing effect on L929 cells under UV irradiation.

4. Conclusions

In summary, core-shell structured TiO_2-SiO_2 nanoparticles of varying shell thicknesses were synthesized and confirmed through SEM and TEM/EDS examinations. FTIR analysis indicated the formation of Ti-O-Si chemical bonds on the surface of TiO_2 nanoparticles. The presence of a silica shell has improved the compatibility of TiO_2 nanoparticles with L929 cells. Both coated and non-coated TiO_2 nanoparticles exhibited good haemocompatibility.

Reduced photocatalytic reactivity was evident after the TiO_2 nanoparticles were coated with silica. This was compensated for by improved cell compatibility. When the silica shell thickness was controlled to a minimum (5.5 nm in this study), the photocatalytic reactivity of coated TiO_2 (TS1) was very close to that of non-coated TiO_2 (P25). The well-maintained photoreactivity of TiO_2 in TS1 was further demonstrated in cellular work in which both P25 and TS1 were able to reduce the viability of L929 cells to below 60% after a 20 min UV irradiation. The nanoparticles have been further modified with various ligands for targeted photodynamic therapy.

Acknowledgements

The authors would like to thank Dr Lihong Liu for her assistance in cell culture work. The technical support by the Centre for Materials Research, Curtin University in operating the SEM and TEM is also acknowledged. The Curtin Electron Microscope Facility is partially funded by the University, State and Commonwealth Governments.

References

[1] T. Matsunaga, R. Tomoda, T. Nakajima and H. Wake, FEMS Microbiol. Lett. 29 (1985) 211.

[2] P. Fernández-Ibáñez, J. Blanco, S. Malato and F.J. Nieves, Water Res. 37 (2003) 3180.

[3] J. Zhu, W. Zheng, B. He, J. Zhang and M. Anpo, J. Mol. Catal. A: Chem. 216 (2004) 35.

[4] A. Fujishima, T.N. Rao and D.A. Tryk, J. Photochem. Photobiol., C 1 (2000) 1.

[5] T. Lopez, E. Ortiz, M. Alvarez, J. Navarrete, J.A. Odriozola, F. Martinez-Ortega, E.A. Páez-Mozo, P. Escobar, K.A. Espinoza and I.A. Rivero, Nanomed Nanotechnol Biol Med 6 (2010) 777.

[6] R.L. Manthe, S.P. Foy, N. Krishnamurthy, B. Sharma and V. Labhasetwar, Mol. Pharmaceutics 7 (2010) 1880.

[7] R. Cai, Y. Kubota, T. Shuin, H. Sakai, K. Hashimoto and A. Fujishima, Cancer Res 52 (1992) 2346.

[8] E. Stefanou, A. Evangelou and P. Falaras, Catal. Today 151 (2010) 58.

[9] Z. Li, L. Mi, P. Wang and J. Chen, Nanoscale Res. Lett. 6 (2011) 1.

[10] J. Xu, Y. Sun, J. Huang, C. Chen, G. Liu, Y. Jiang, Y. Zhao and Z. Jiang, Bioelectrochemistry 71 (2007) 217.

[11] T.J. Yoon, K.N. Yu, E. Kim, J.S. Kim, B.G. Kim, S.H. Yun, B.H. Sohn, M.H. Cho, J.K. Lee and S.B. Park, Small 2 (2006) 209.

[12] R.L. Pozzo, M.A. Baltanás and A.E. Cassano, Catal. Today 39 (1997) 219.

[13] S. Pazokifard, S.M. Mirabedini, M. Esfandeh, M. Mohseni and Z. Ranjbar, Surf. Interface Anal. 44 (2012) 41.

[14] R. Han, M. Yu, Q. Zheng, L. Wang, Y. Hong and Y. Sha, Langmuir 25 (2009) 12250.

[15] A. Teleki, M. Suter, P.R. Kidambi, O. Ergeneman, F. Krumeich, B.J. Nelson and S.E. Pratsinis, Chem. Mater. 21 (2009) 2094.

[16] D.A. Mbeh, R. França, Y. Merhi, X.F. Zhang, T. Veres, E. Sacher and L. Yahia, J. Biomed. Mater. Res., Part A 100A (2012) 1637.

[17] G. Carturan, R. Dal Toso, S. Boninsegna and R. Dal Monte, J. Mater. Chem. 14 (2004) 2087.

[18] I.A. Siddiquey, T. Furusawa, M. Sato, N.M. Bahadur, M. Mahbubul Alam and N. Suzuki, Ultrason. Sonochem. 19 (2012) 750.

[19] A.M. Eltoni, S. Yin, T. Sato, T. Ghannam, M. Al Hoshan and M. Al Salhi, J. Alloys Compd. 508 (2010) L1.

[20] H. Sun, X. Feng, S. Wang, H.M. Ang and M.O. Tadé, Chem. Eng. J. 170 (2011) 270.

[21] F. Erogbogbo, K.T. Yong, I. Roy, G. Xu, P.N. Prasad and M.T. Swihart, ACS Nano 2 (2008) 873.

[22] C.H. Ahn, S.Y. Chae, Y.H. Bae and S.W. Kim, J. Controlled Release 97 (2004) 567.

[23] X. He, X. Wu, X. Cai, S. Lin, M. Xie, X. Zhu and D. Yan, Langmuir 28 (2012) 11929.

[24] K. Ogura, K. Nakaoka, M. Nakayama, M. Kobayashi and A. Fujii, Anal. Chim. Acta 384 (1999) 219.

[25] R. Hong, T. Pan, J. Qian and H. Li, Chem. Eng. J. 119 (2006) 71.

[26] I.A. Siddiquey, T. Furusawa, M. Sato and N. Suzuki, Mater. Res. Bull. 43 (2008) 3416.

[27] M. José Velasco, F. Rubio, J. Rubio and J.L. Oteo, Thermochim. Acta 326 (1999) 91.

[28] M. Crişan, A. Brăileanu, M. Răileanu, M. Zaharescu, D. Crişan, N. Drăgan, M. Anastasescu, A. Ianculescu, I. Nițoi, V.E. Marinescu and S.M. Hodorogea, J. Non-Cryst. Solids 354 (2008) 705.

[29] H. Sun, Y. Bai, H. Liu, W. Jin and N. Xu, J. Photochem. Photobiol., A 201 (2009) 15.

Figure Captions

Fig. 1. FESEM micrographs of P25 and TS1-4.

Fig. 2. TEM images of P25 and TS1 (Left), showing the core-shell structure of TS1. EDS of TS1 (Right), showing the presence of elemental Ti, Si and O. Cu is from the copper grid and C is from both TS1 and the carbon film coated on the copper grid.

Fig. 3. FTIR spectra for P25 and TS1-4.

Fig. 4. Phenol concentration change with time (Insert: degradation rate change with shell thickness).

Fig. 5. Cell viability after treatment with P25, TS1 and TS4 for (a) 6 h and (b) 24 h.
*$p<0.05$ as compared to control (untreated) cells.
**$p<0.05$ as compared to the P25 treated cells.
All data are expressed as the mean ± SD and n=3.

Fig. 6. Light micrographs of L929 cells treated with (a) no nanoparticles, (b) P25, (c) TS1, and (d) TS4. Incubation time = 24 h. The nanoparticle concentration = 200 μg/ml.

Fig. 7. Haemolysis assays of P25, TS1 and TS4 nanoparticles.
All data are expressed as the mean ± SD and n=3.

Fig. 8. Effect of UV irradiation time on viability of L929 cells.
*$p<0.05$ as compared to cells without UV irradiation.
All data are expressed as the mean ± SD and n=4.

Fig. 9. Effect of photo-excited TiO_2 and TiO_2-SiO_2 nanoparticles on cell viability. Irradiation time was 20 min.
*$p<0.05$ as compared to control.
All data are expressed as the mean ± SD and n=4.

Figure(s)

Fig. 1.

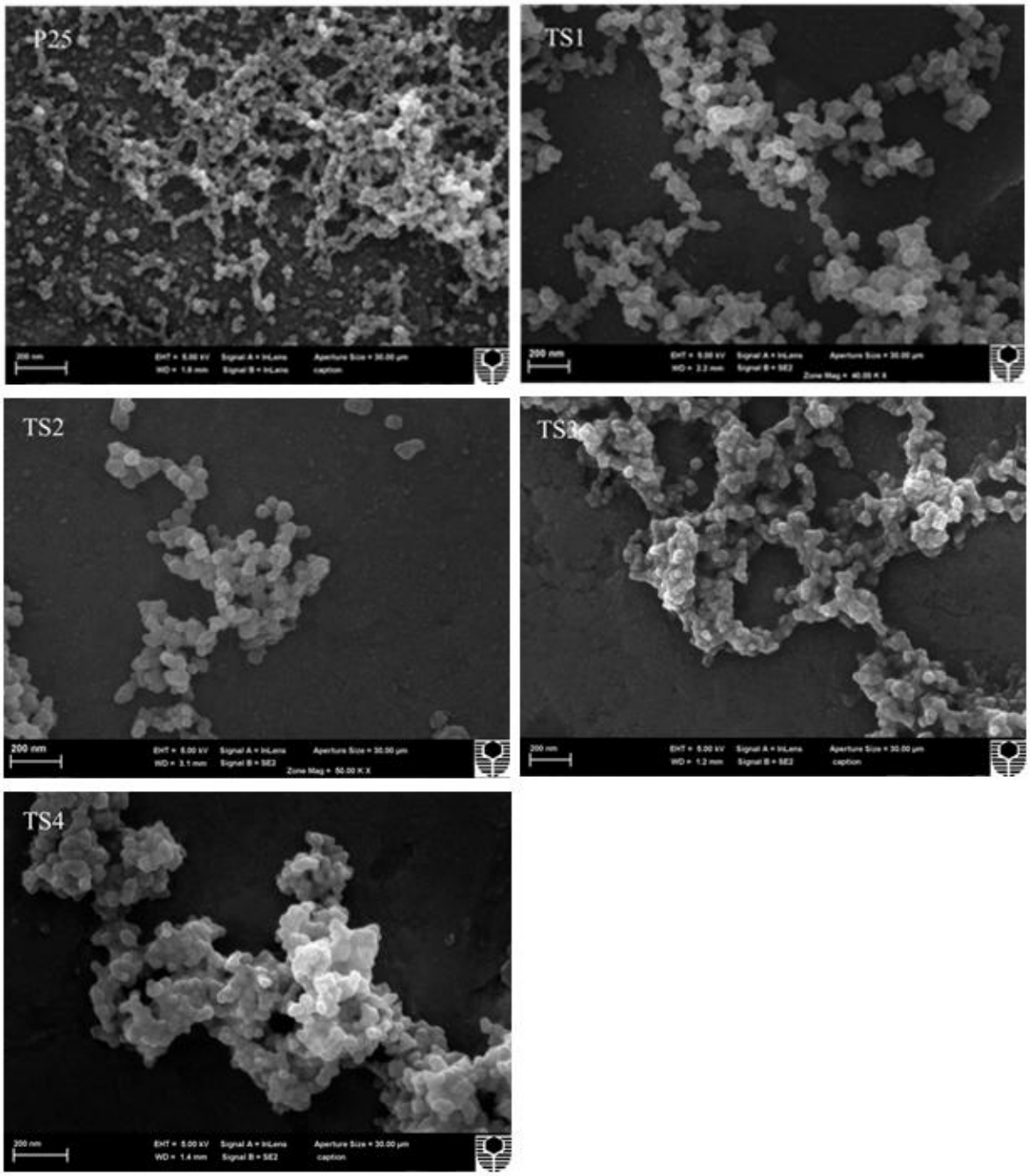

Fig. 2.

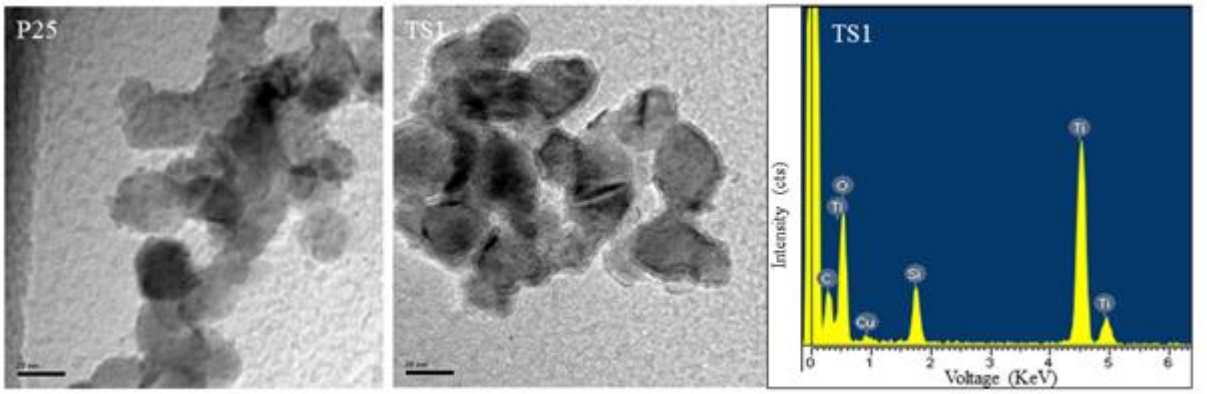
P25
TS1
TS1
Intensity (cts)
O
Ti
C
Cu
Si
Ti
Ti
0
1
2
3
4
5
6
Voltage (KeV)

Fig. 3.

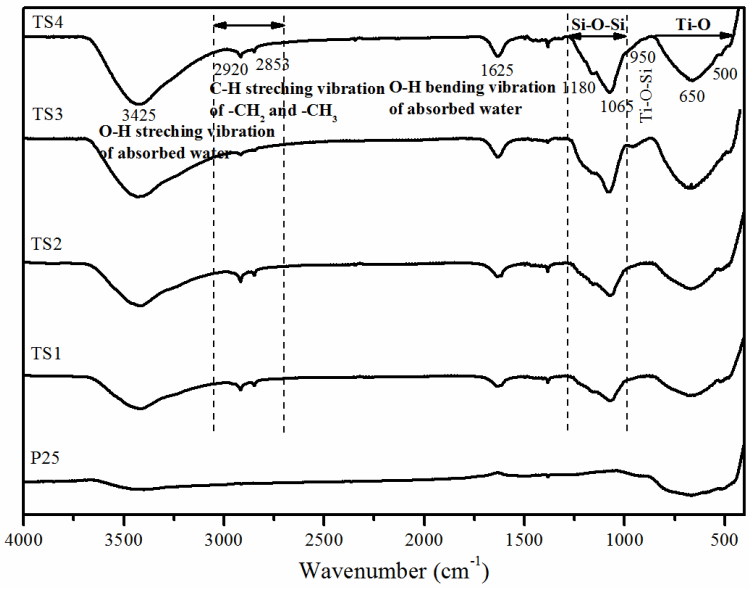
TS4
TS3
TS2
TS1
P25
3425
O-H streching vibration
of absorbed water
2920
2853
C-H streching vibration
of -CH2 and -CH3
1625
O-H bending vibration
of absorbed water
Si-O-Si
1180
1065
950
Ti-O-Si
Ti-O
650
500
4000
3500
3000
2500
2000
1500
1000
500
Wavenumber (cm-1)

Fig. 4.

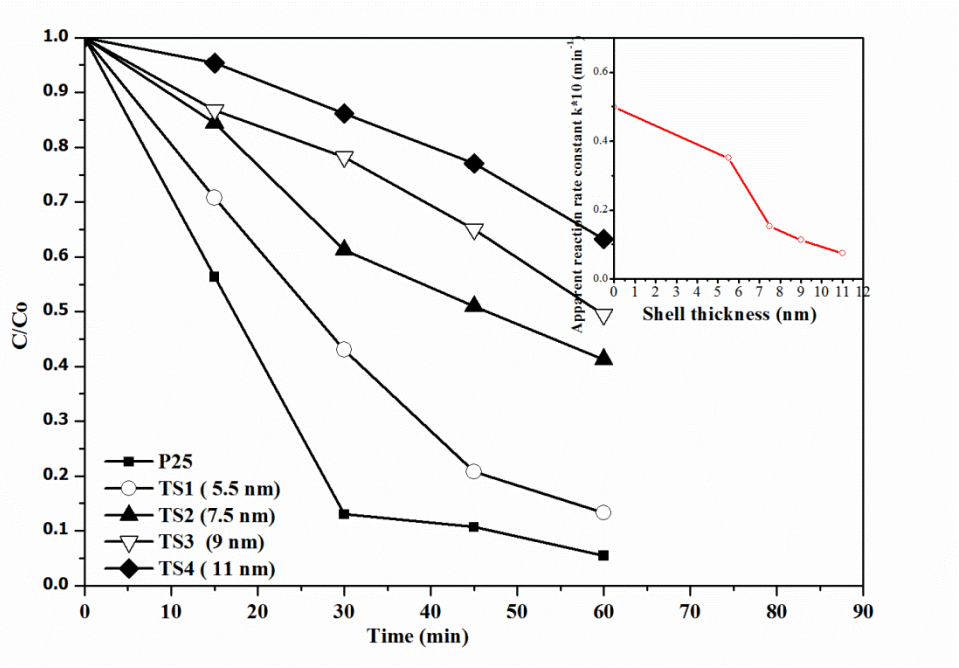
C/Co
Time (min)
P25
TS1 (5.5 nm)
TS2 (7.5 nm)
TS3 (9 nm)
TS4 (11 nm)
Apparent reaction rate constant k*10 (min-1)
Shell thickness (nm)

Fig. 5.

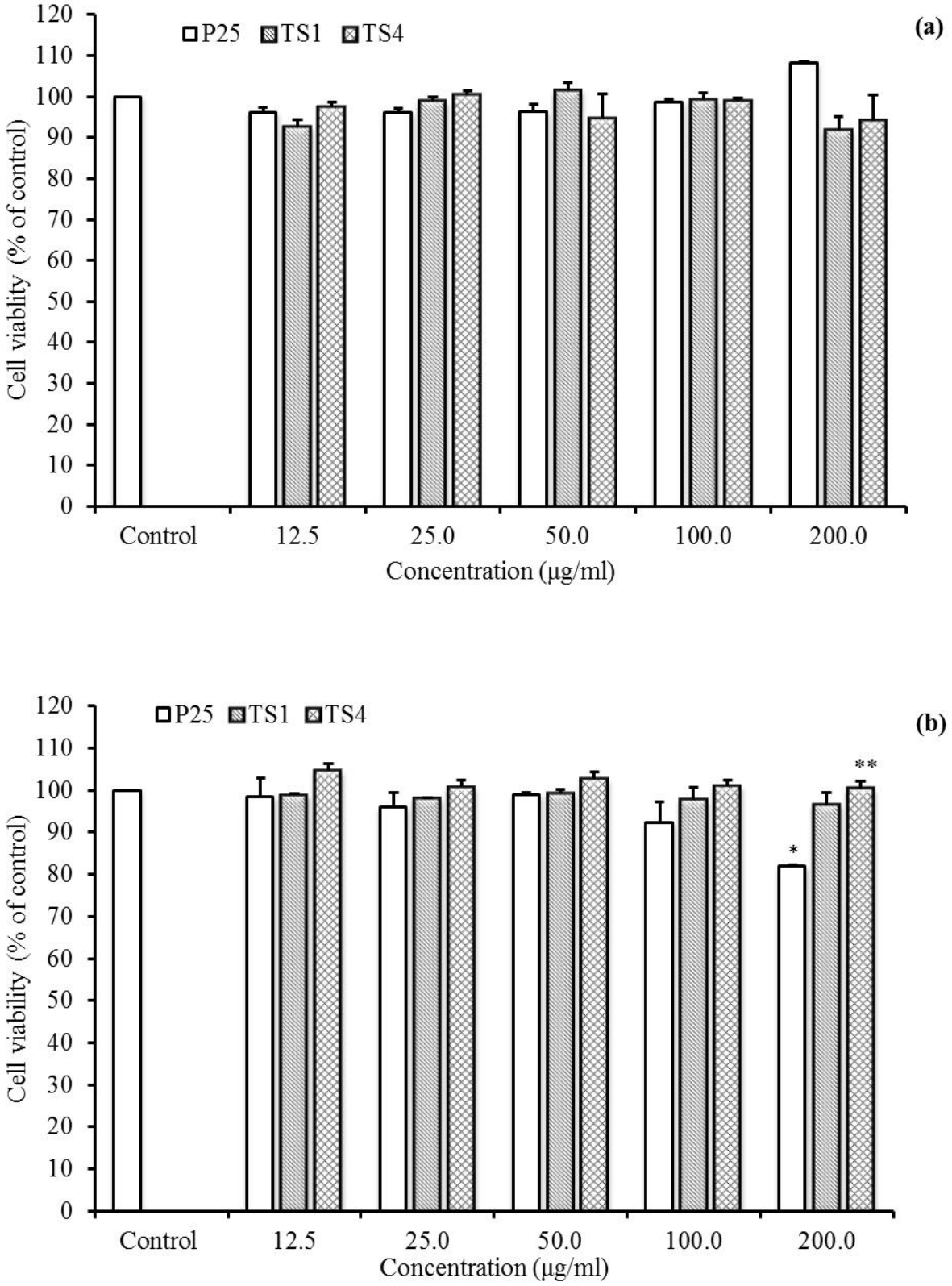
(a)
P25
TS1
TS4
Cell viablity (% of control)
120
110
100
90
80
70
60
50
40
30
20
10
0
Control
12.5
25.0
50.0
100.0
200.0
Concentration (µg/ml)
(b)
P25
TS1
TS4
Cell viability (% of control)
*
**
Control
12.5
25.0
50.0
100.0
200.0
Concentration (µg/ml)

Fig. 6.

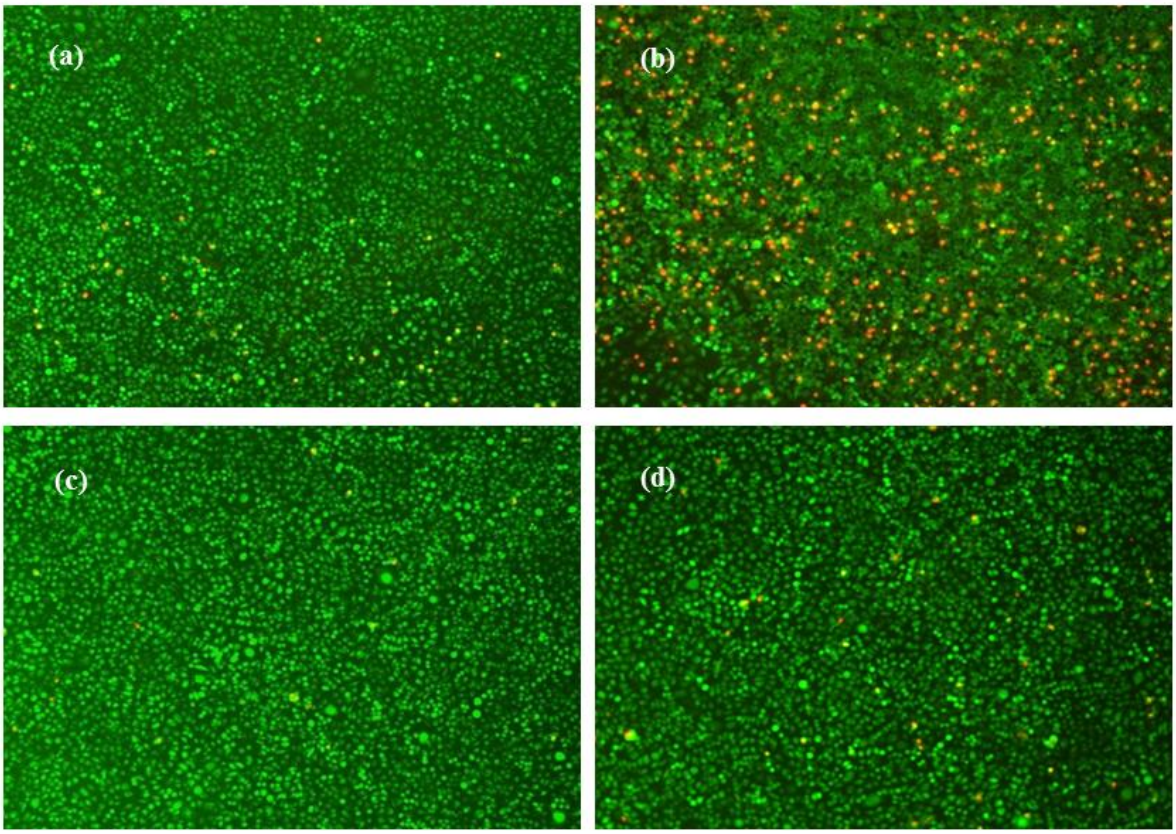

Fig. 7.

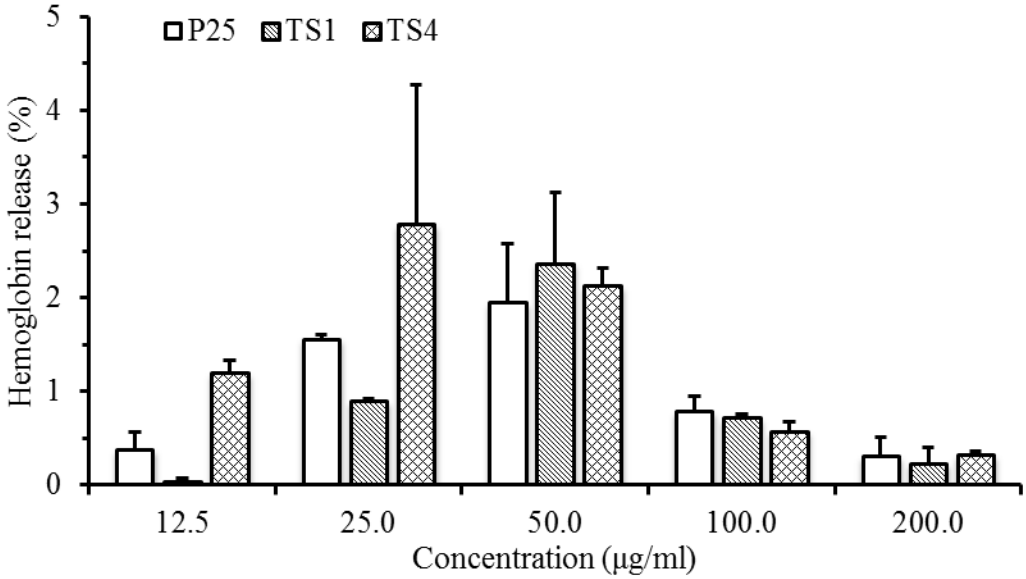
P25
TS1
TS4
Hemoglobin release (%)
0
1
2
3
4
5
12.5
25.0
50.0
100.0
200.0
Concentration (µg/ml)

Fig. 8.

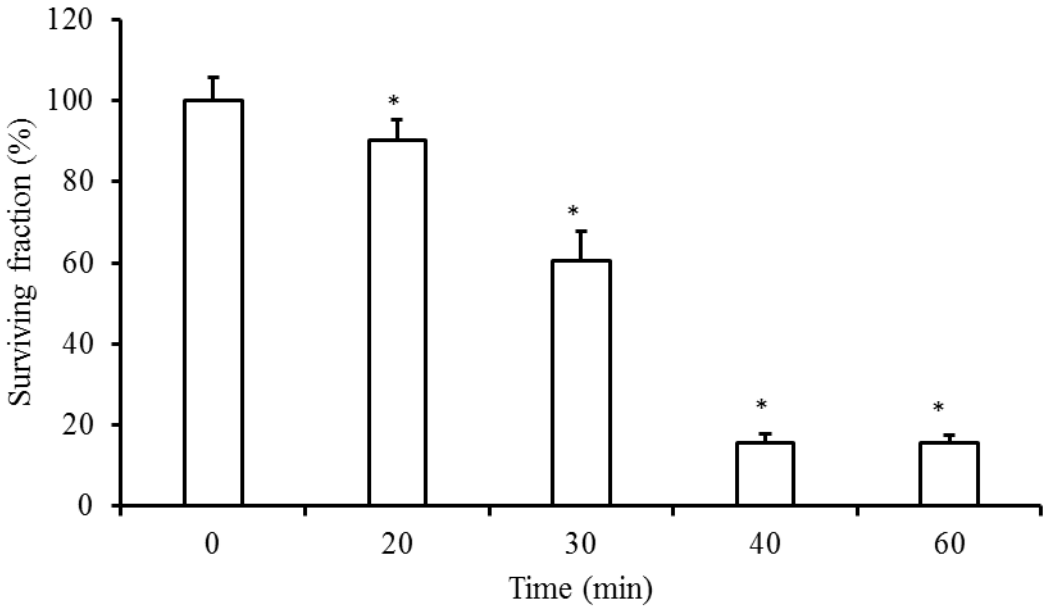

Fig. 9.

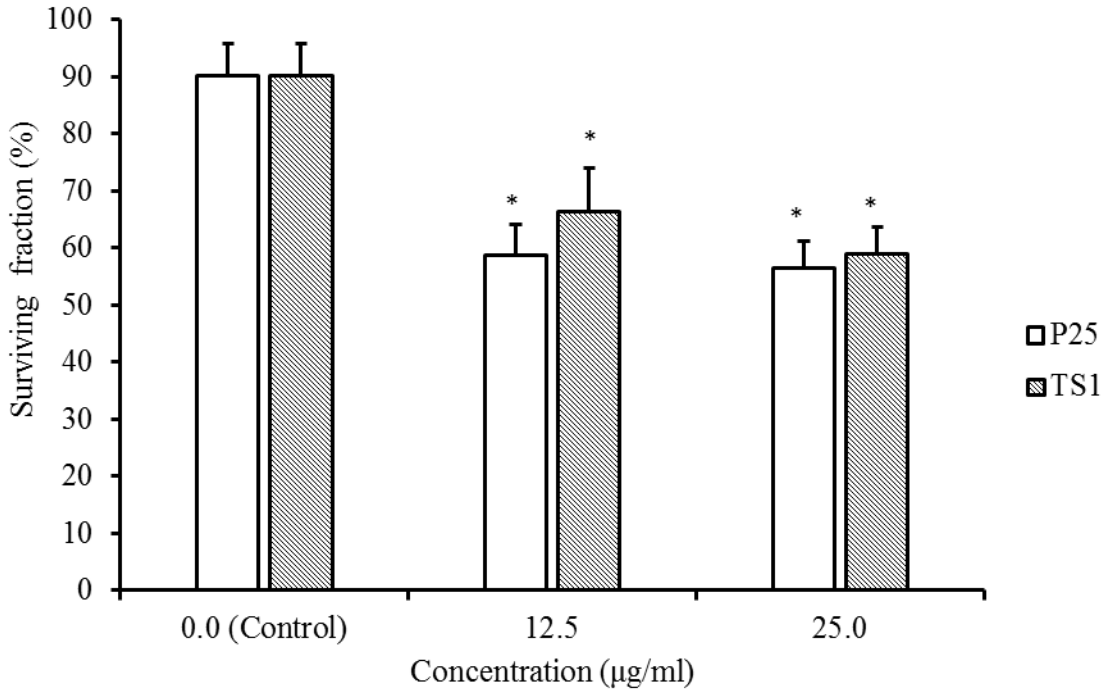
100
90
80
70
60
50
40
30
20
10
0
Surviving fraction (%)
*
*
*
*
0.0 (Control)
12.5
25.0
Concentration (µg/ml)
P25
TS1